Spectral Viscosity for Shallow Water Equations in Spherical Geometry

ANNE GELB AND JAMES P. GLEESON

Department of Mathematics, Arizona State University, Tempe, Arizona

(Manuscript received 13 July 2000, in final form 20 February 2001)

ABSTRACT

A spherical spectral viscosity operator is proposed as an alternative to standard horizontal diffusion terms in global atmospheric models. Implementation in NCAR's Spectral Transform Shallow Water Model and application to a suite of standard test cases demonstrates improvement in resolution and numerical conservation of invariants at no extra computational cost. The retention in the spectral viscosity solution of high-wavenumber information allows the successful application of high-resolution postprocessing methods.

1. Introduction

The numerical solution of the shallow water equations of global atmospheric models provides a challenging computational problem, involving motion on widely disparate space and time scales. A variety of numerical methods have been proposed; see, for example, Gottelmann (1999), Hack (1992), Spotz et al. (1998), Swarztrauber (1996), and Taylor et al. (1997). Among these, spectral methods are very popular, chiefly because of their high accuracy and the absence of the ''pole problem,'' which arises in standard finite-difference schemes (Orszag 1974). The spectral transform method pioneered by Orszag (1970) and Eliasen et al. (1970) uses fast Fourier transforms to evaluate nonlinear terms to increase the cost effectiveness of these methods, making them competitive with finite-difference schemes. One major drawback of spectral methods is the occurrence of the Gibbs phenomenon when discontinuities or sufficiently high gradients develop in the fluid variables. The Gibbs phenomenon is characterized by the appearance of spurious oscillations in physical space and a reduction of global accuracy to first order. Another problem is manifested in spectral space, for example in the kinetic energy spectrum. The nonlinear evolution equations generate an energy cascade from lower-to higher-wavenumber modes, and in underresolved calculations the energy builds up at the truncation limit, creating a spectrum with an erroneously high tail—the so called spectral blocking problem.

The traditional approach to dealing with these difficulties in the spectral method is to add an artificial diffusion term (called the horizontal diffusion term in numerical models) to the equations of motion, typically a second- or fourth-order derivative in the space variables. This small viscouslike term smears the discontinuities or high gradients over several grid points and allows the smeared solution to be well resolved by the truncated spectral series. As a result the spurious Gibbs phenomenon oscillations (also known as spectral ringing) are eliminated. The artificial diffusion term dissipates energy, and this effect may be tuned so that the tails of the energy spectrum do not exhibit the spectral blocking problem.

Nevertheless, the use of artificial diffusion is not without problems. Chief among these is the excessive smearing of underresolved calculations, leading to the loss of information on the detailed structure of the fluid flow. Due to the cost of high-resolution calculations, it is desirable that the basic flow structure should be calculated as accurately as possible even when the flow is underresolved. The physical scales corresponding to wavenumber modes beyond the truncation limit are commonly referred to as ''subgrid'' scales. Artificial diffusion terms are often justified in a more or less ad hoc manner as representing the process of mixing by the unresolved subgrid scales. Attempts at rigorous modeling of the effect of subgrid scales have had various degrees of success; see, for example, the review by Lesieur and Metais (1996). One important realization is that the damping of low-wavenumber modes by standard diffusion terms is excessive and is the major source of the errors mentioned above. For example, the horizontal diffusion term in the global climate model of Bourke et al. (1977) is applied only to wavenumber modes above a cutoff, which is (arbitrarily) chosen to be half of the truncation limit. Leith (1971) applied a turbulence closure theory to approximate the subgrid-scale effects upon the resolved scales in a two-dimensional Cartesian

Corresponding author address: James Gleeson, Applied Mathematics, University College Cork, Cork, Ireland.
E-mail: gleeson@math.la.asu.edu

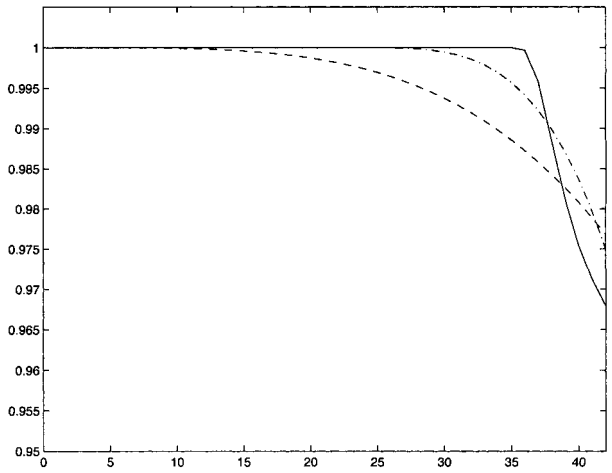

FIG. 1. Filters vs wavenumber n for $M = 42$ artificial diffusion σ_n (dashed), spectral viscosity σ_n^{SV} (solid), and Leith diffusion σ_n^L (dot–dash).

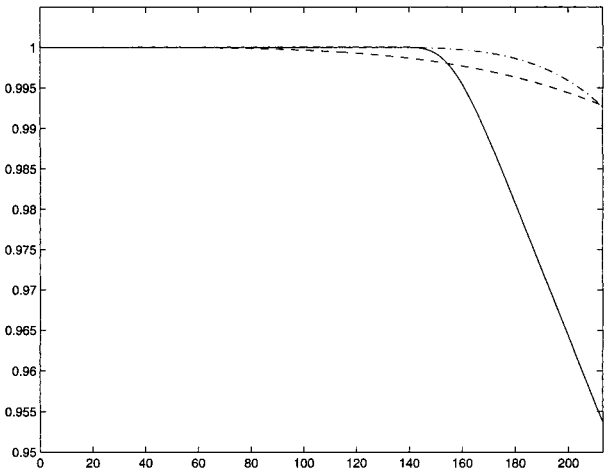

FIG. 2. Filters vs wavenumber n for $M = 213$: artificial diffusion σ_n (dashed), spectral viscosity σ_n^{SV} (solid), and Leith diffusion σ_n^L (dot–dash).

model of the atmosphere. He derived an eddy-viscosity term by assuming the existence of a steady enstrophy-cascading -3 power spectrum. This eddy viscosity has been adapted in several numerical models for flows on the sphere, by means of a horizontal diffusion term that is zero for wavenumbers less than 55% of the total wavenumber. In this paper we apply a spectral viscosity (SV) method, which is motivated by rigorous mathematical results for nonlinear conservation laws, and yields a viscosity term that, like Leith's, depends upon wavenumber and is equal to zero for low wavenumbers. However the cutoff wavenumber and the form of the nonzero diffusion are quite different.

The SV method was introduced by Tadmor (see Tadmor 1989; Maday and Tadmor 1989; Chen et al. 1993; Maday et al. 1993). The idea is to replace the artificial diffusion term with a nonlocal viscosity-like term in spectral space. It has been shown that the use of the SV method yields convergence to the correct entropy solution of nonlinear conservation laws, with spectral accuracy recoverable away from discontinuities (and even up to the discontinuities with appropriate postprocessing methods). Particular advantages of the SV method are its retention of high-wavenumber information and consequent lack of excessive smearing. Furthermore, the SV result allows the use of a high-resolution postprocessing method that is then able to recover the finer features of the solution (Gelb and Tadmor 2000). The SV method has been applied in numerical calculations of the Euler equations of gas dynamics (Maday et al. 1993) and to the shallow water equations in one and two Cartesian dimensions by the current authors. Karamanos and Karniadakis (1999) employed a SV-type term to model subgrid mixing in their finite-element calculations of incompressible Navier–Stokes flow, and Andreassen et al. (1994) use spectral viscosity to stabilize their two-dimensional simulations of atmospheric gravity waves. In this paper we derive an SV term for spherical geometry and apply it to shallow water flow with earthlike parameters. The shallow water equations on the sphere present many of the difficulties associated with the horizontal component of three-dimensional atmospheric modeling, and so they provide a first test for numerical schemes applicable to full-scale global models.

The suite of test problems proposed by Williamson et al. (1992) has become an accepted benchmark for numerical methods applied to the shallow water equations on the sphere. Jakob-Chien et al. (1995) provide a spectral transform shallow water model (STSWM) code to solve the test suite. They adopt a standard artificial diffusion term and obtain accurate results for height and wind fields at sufficiently high resolution. However, as demonstrated here, the use of a spectral viscosity term is preferable to artificial diffusion in cases that are underresolved, while still reproducing the excellent results of Jakob-Chien et al. (1995) when resolution is increased. Moreover, the use of SV improves the conservation of invariants by the numerical scheme, yields more accurate energy spectra, and permits the use of postprocesing methods to yield high-resolution solutions. These numerical results are presented in section 4 and are preceded by discussion of the shallow water equations and STSWM code in section 2 and the spectral viscosity method in section 3. In section 5 we discuss the application of SV to parameter tuning in models where Leith's diffusion term is already employed.

2. Shallow water equations and STSWM implementation

We briefly review here the equations and implementation by Jakob-Chien et al. (1995) of the STSWM. For further details consult Jakob-Chien et al. (1995), Jakob et al. (1993), and Hack and Jakob (1992).

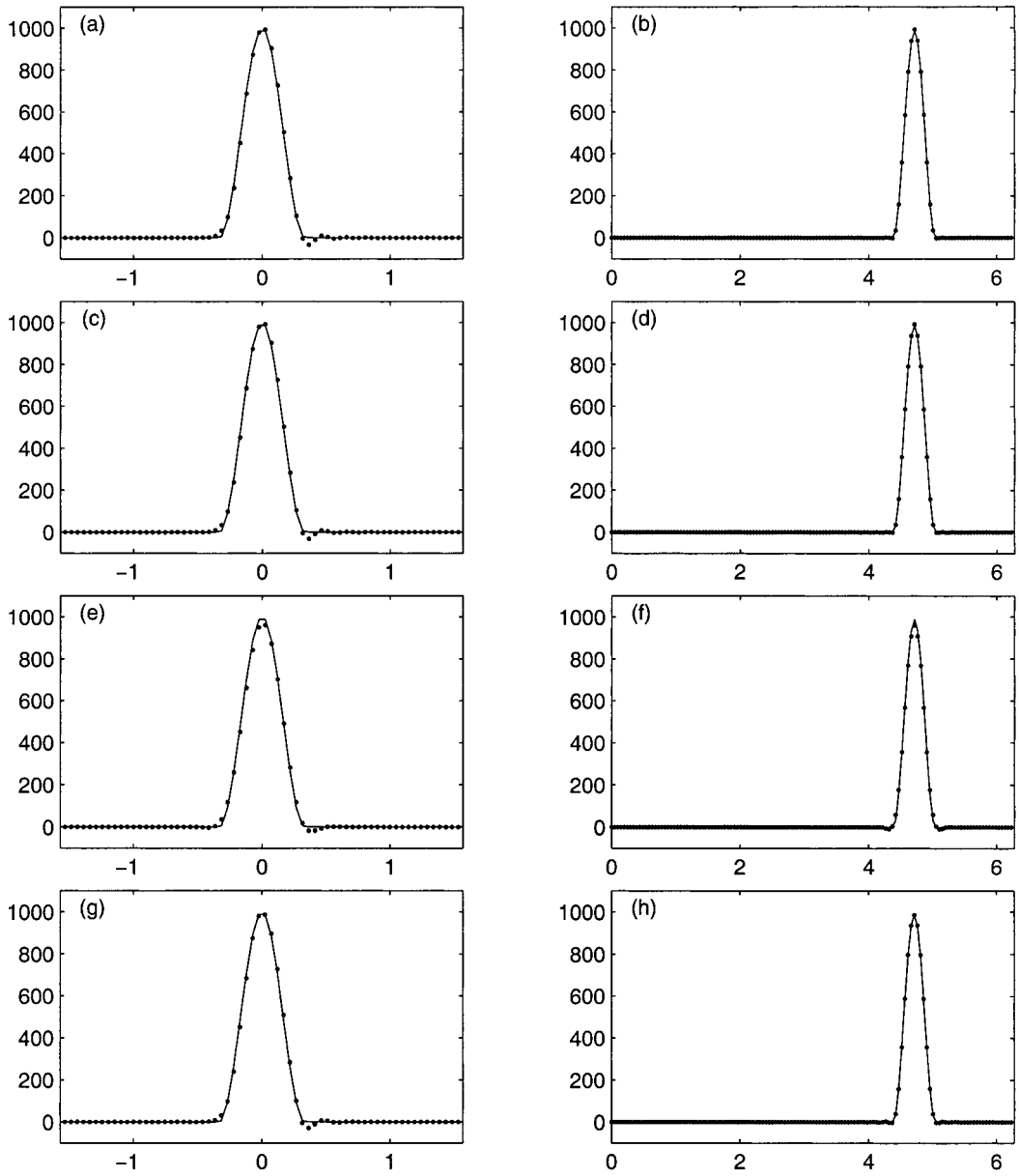

FIG. 3. Exact (solid line) and numerical (dots) height field for test case 1 after one rotation: (a), (b) no diffusion, (c), (d) spectral viscosity, (e), (f) artificial diffusion, and (g), (h) Leith diffusion. Constant longitude cross sections on left and constant latitude on right.

The shallow water equations on a sphere may be written in vector form as

$$\frac{d}{dt}\mathbf{V} = -f\mathbf{k} \times \mathbf{V} - \nabla(\phi + \phi_s), \tag{1}$$

$$\frac{d}{dt}\phi = -\phi\nabla \cdot \mathbf{V}, \tag{2}$$

where $\mathbf{V}$ is the vector velocity parallel to the surface of the sphere, $\mathbf{k}$ is the outward radial unit vector, f is the Coriolis parameter, $\phi = gh$ is the geopotential of the fluid of depth h, and ϕ_s is the surface geopotential gh_s. Scalar equations for the absolute vorticity $\eta \equiv \mathbf{k} \cdot \nabla \times \mathbf{V} + f$, the divergence $\delta \equiv \nabla \cdot \mathbf{V}$, and the variation of the geopotential ϕ' from its spatial mean $\overline{\phi}(\phi' = \phi - \overline{\phi})$ are found by applying the curl and divergence operators to (1):

$$\frac{\partial \eta}{\partial t} = -\frac{1}{a(1-\mu^2)}\frac{\partial}{\partial \lambda}(U\eta) - \frac{1}{a}\frac{\partial}{\partial \mu}(V\eta) + F_\eta, \tag{3}$$

$$\frac{\partial \delta}{\partial t} = \frac{1}{a(1-\mu^2)}\frac{\partial}{\partial \lambda}(V\eta) - \frac{1}{a}\frac{\partial}{\partial \mu}(U\eta) - \nabla^2\left(\phi_s + \phi' + \frac{U^2 + V^2}{2(1-\mu^2)}\right) + F_\delta, \tag{4}$$

$$\frac{\partial \phi'}{\partial t} = -\frac{1}{a(1-\mu^2)}\frac{\partial}{\partial \lambda}(U\phi') - \frac{1}{a}\frac{\partial}{\partial \mu}(V\phi') - \overline{\phi}\delta + F_\phi. \quad (5)$$

Here a is the radius of the earth, λ is the longitude, and $\mu = \sin\theta$ where θ is the latitude. The components of the velocity vector have been written in the form.

$$\mathbf{V} = \frac{U}{\cos\theta}\mathbf{i} + \frac{V}{\cos\theta}\mathbf{j},$$

where the variables $U = u\cos\theta$ and $V = v\cos\theta$ are used for calculation because they are better suited to scalar spectral expansions than the pseudoscalar wind components u and v (see Robert 1966). Artificial diffusion terms have been added to the right-hand side of the equations; Jakob-Chien et al. (1995) choose these to have the form of the horizontal diffusion used in the National Center for Atmospheric Research (NCAR) community climate models:

$$F_\eta = -K_4\left(\nabla^4\eta - \frac{4}{a^4}\eta\right), \quad (6)$$

$$F_\delta = -K_4\left(\nabla^4\delta - \frac{4}{a^4}\delta\right), \quad (7)$$

$$F_\phi = -K_4\nabla^4(\phi + \phi_s), \quad (8)$$

with a resolution-dependent diffusion coefficient K_4. These terms are of the form discussed in section 1, with linear corrections to the fourth-order derivative in (6) and (7) to avoid damping solid-body rotation (see Bourke et al. 1977; Orszag 1974), and the surface geopotential in (8) to avoid extra damping due to surface topography.

The spectral transform is applied to solve equations (3)–(5). Each variable is expanded on a spherical harmonic basis; for example, the absolute vorticity is written as

$$\eta(\lambda, \mu) = \sum_{m=-M}^{M}\sum_{n=|m|}^{M}\eta_n^m P_n^m(\mu)e^{im\lambda}. \quad (9)$$

The associated Legendre functions are denoted $P_n^m(\mu)$ and a triangular spectral truncation of order M has been chosen. The spectral coefficients η_n^m are found from the grid values $\eta(\lambda_i, \mu_j)$, $i = 1, \ldots, I$, and $j = 1, \ldots, J$ using a fast Fourier transform in λ and a Gaussian quadrature approximation on the J roots of $P_J^0(\mu) = 0$. The truncation order M is related to the number of grid points in the longitudinal and meridional directions by

$$I \geq 3M + 1, \quad \text{and} \quad J \geq \frac{1}{2}(3M + 1),$$

respectively. See Table I of Jakob-Chien et al. (1995) for values of M, I, and J used in numerical calculations, and Table III of Jakob-Chien et al. (1995) for values of the diffusion coefficient K_4. These scale as $M^{-2}(M + 1)^{-2}$ for increasing M.

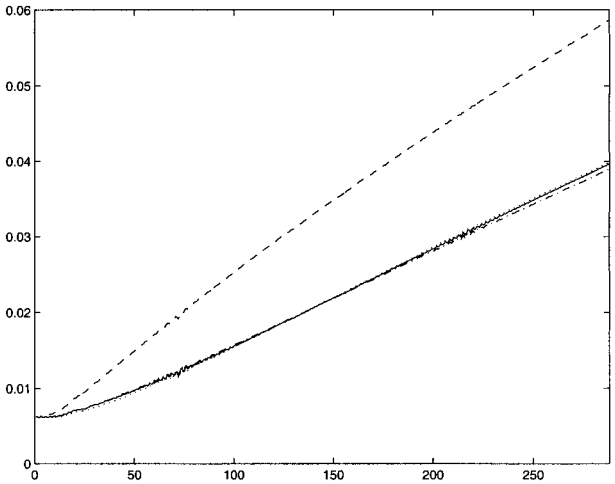

FIG. 4. T42 global L_2 error norms for test case 1 vs time in h: no diffusion (dotted), spectral viscosity (solid), artificial diffusion (dashed), and Leith diffusion (dot–dash).

Equations (3)–(5) are transformed into prognostic equations for the spectral coefficients η_n^m, δ_n^m, and $\phi_n'^m$. A semi-implicit time-stepping procedure is used to treat gravity waves implicitly and remaining terms explicitly, thus increasing the Courant–Freidrichs–Levy limit on the time step. At each time step the spectral coefficients are first determined from the prognostic equations with the diffusion terms omitted to give intermediate values $\tilde{\eta}_n^m$, $\tilde{\delta}_n^m$, and $\tilde{\phi}_n'^m$. The diffusion terms (6)–(8) are then included in an implicit fashion (see Jakob et al. 1993), by solving

$$\eta_n^m = \tilde{\eta}_n^m - 2\Delta t K_4\frac{n^2(n+1)^2 - 4}{a^4}\eta_n^m \quad (10)$$

for the new value η_n^m, and similarly for the other variables. Note that (10) may be rewritten as

$$\eta_n^m = \sigma_n\tilde{\eta}_n^m, \quad (11)$$

$$\sigma_n = \frac{1}{1 + 2\Delta t K_4\dfrac{n^2(n+1)^2 - 4}{a^4}}. \quad (12)$$

Hence the artificial diffusion is equivalent to applying a spectral filter of form σ_n at each time step (Canuto et al. 1987).

3. Spectral viscosity

Spectral viscosity regularization was first introduced by Tadmor (1989) with a view to stabilizing numerical solutions of nonlinear hyperbolic systems such as Burgers' equation and the Euler equations of gas dynamics. Discontinuities in the fluid variables arise naturally in these systems and lead to the familiar Gibbs phenom-

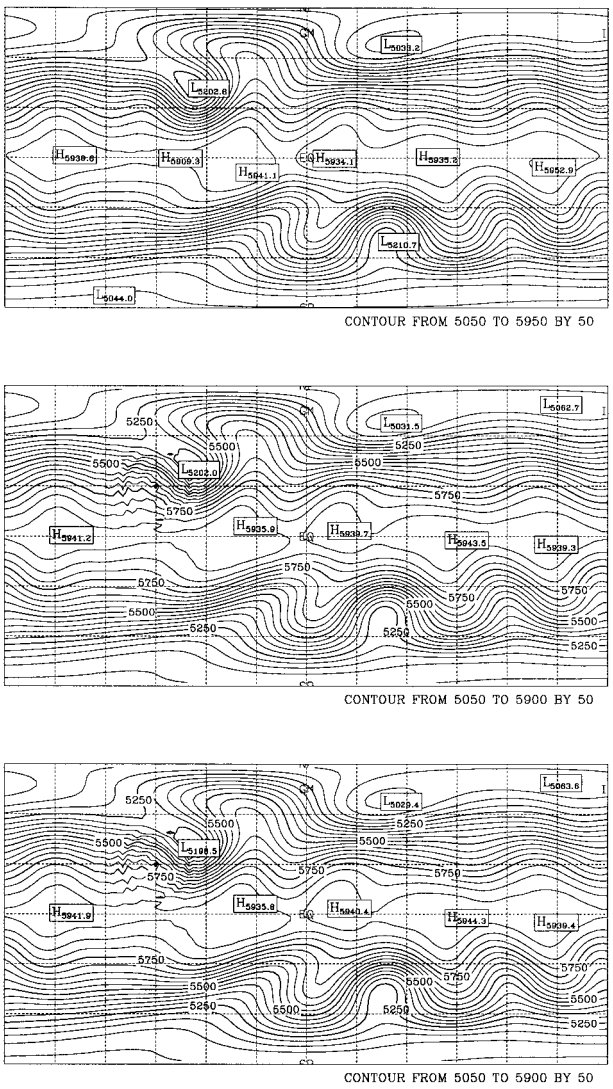

FIG. 5. Height field for flow over a conical mountain: (a) T213 reference, (b) artificial diffusion, and (c) spectral viscosity.

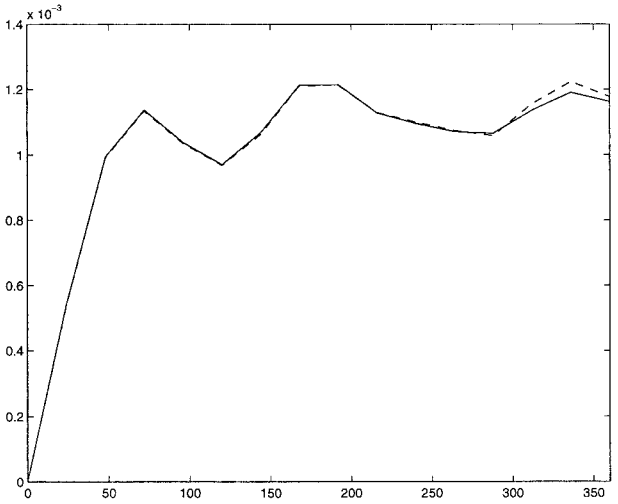

FIG. 6. L_2 errors vs time in h for T42 flow over a conical mountain, using artificial diffusion (dashed) and spectral viscosity (solid).

enon when solved using spectral methods, and to possible instabilities. Artificial diffusion terms in the form of second- or fouth-order spatial derivatives may be introduced to maintain stability, but at the expense of smearing the discontinuity and losing information on the shock location. This information is vital for the application of cosmetic postprocessing methods, which are capable of yielding very accurate solutions (see Gelb and Tadmor 2000). The spectral viscosity (more correctly called the spectral vanishing viscosity) operator replaces the artificial diffusion by a term that acts only on high wavenumbers, that is, on the small scales. Tadmor and coworkers have shown that this SV term is sufficient to retain stability in the calculation, but because it does not affect low-wavenumber modes it has significantly less smearing effect. In particular, SV solutions retain sufficient information to allow for (automatic) detection of discontinuities and hence the application of high-resolution postprocessing reconstruction methods (Gelb and Tadmor 2000).

We consider in this section the replacement of the standard artificial diffusion terms (6)–(8) by appropriate SV terms and demonstrate (in section 4) the superiority of the SV method with regard to reduced smearing of height and wind fields, amelioration of spectral blocking, and improved conservation of kinetic energy and potential enstrophy.

We defer to the appendix the mathematical derivation of an appropriate SV term on the sphere and merely note here that the result may be considered a generalization of the standard diffusion terms, for example, as in (6):

$$F_\eta = -K_4\nabla^4\eta, \tag{13}$$

where for clarity we ignore for now the correction for solid-body rotation. The simplest form for an isotropic spherical harmonic (super) spectral viscosity term is [see Eq. (A2)]

$$F_\eta^{\mathrm{SV}} = -\epsilon Q\nabla^4(Q\eta), \tag{14}$$

with corresponding terms for the other variables:

$$F_\delta^{\mathrm{SV}} = -\epsilon Q\nabla^4(Q\delta) \quad \text{and} \tag{15}$$

$$F_\phi^{\mathrm{SV}} = -\epsilon Q\nabla^4[Q(\phi + \phi_s)]. \tag{16}$$

Here Q is a nonlocal operator that is defined by

$$Q\psi = \sum_{m=-M}^{M}\sum_{n=|m|}^{M}\hat{q}_n\psi_n^m P_n^m(\mu)e^{im\lambda} \tag{17}$$

and ψ has the spherical harmonic expansion

$$\psi = \sum_{m=-M}^{M}\sum_{n=|m|}^{M}\psi_n^m P_n^m(\mu)e^{im\lambda}. \tag{18}$$

The spectral viscosity coefficients $\hat{q}_n$ are zero for low

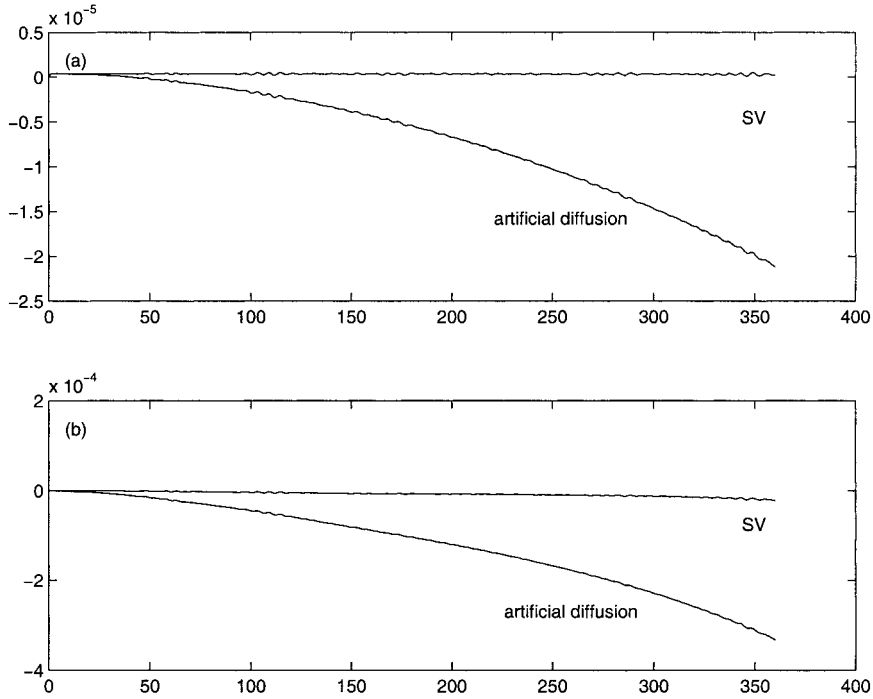

FIG. 7. Global conservation integrals for T42 flow over a conical mountain, using artificial diffusion and spectral viscosity: (a) normalized total energy and (b) normalized potential enstrophy.

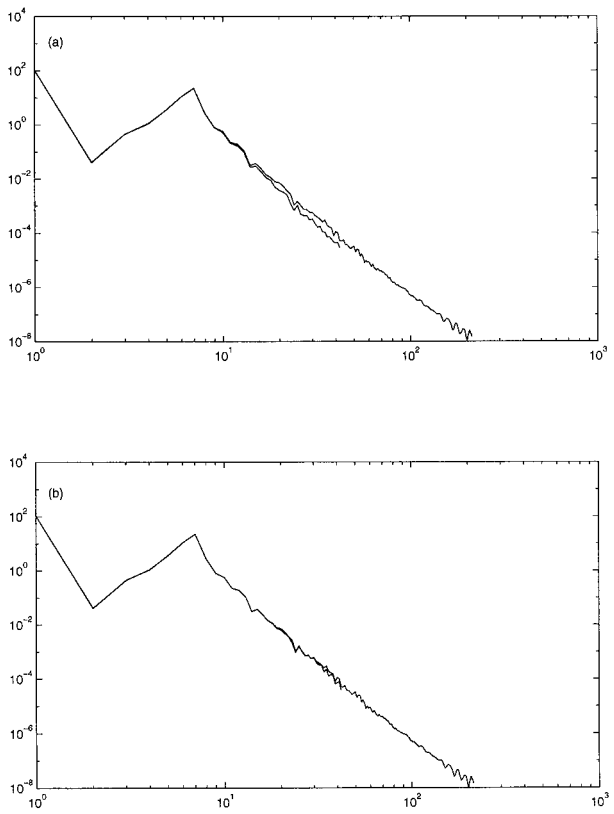

FIG. 8. Kinetic energy spectra for day 15 of flow over a conical mountain: (a) T213 reference solution and T42 artificial diffusion and (b) T213 reference solution and T42 spectral viscosity.

wavenumbers n and rise to one as n approaches the truncation limit M. A typical smooth choice for the SV coefficients is given by (see Maday et al. 1993)

$$\hat{q}_n = \begin{cases} 0 & n \le n_c, \\ \exp\left[-\dfrac{(n-M)^2}{2(n-n_c)^2}\right] & n_c < n \le M. \end{cases} \tag{19}$$

The SV amplitude ϵ and cutoff n_c depend upon the truncation order M; as M increases, ϵ decreases and n_c increases. Proofs of spectral convergence (Tadmor 1993; Ma 1998) use power-law dependence of ϵ and n_c upon M; for example,

$$\epsilon \sim \frac{1}{M^3}, \qquad n_c \sim M^{3/4}. \tag{20}$$

The diffusion term (6) has spectral coefficients

$$\{F_\eta\}_n^m = -K_4 \frac{n^2(n+1)^2}{a^4}\eta_n^m, \tag{21}$$

and the corresponding SV term (14) has coefficients

$$\{F_\eta^{\mathrm{SV}}\}_n^m = -\epsilon \hat{q}_n^2 \frac{n^2(n+1)^2}{a^4}\eta_n^m. \tag{22}$$

The improved results from using the SV terms all arise from the fact that $\hat{q}_n$ is a function of n, in contrast to the constant value of K_4 in (21). Note that the SV term (14) reduces to the standard diffusion form (13) if $\hat{q}_n \equiv 1$. The fact that the SV term is zero for low wave-

numbers $n < n_c$ reduces the undesirable smearing while the high wavenumbers are damped to reduce Gibbs oscillations and spectral blocking.

a. Implementation of SV in STSWM code

Modification of the STSWM code to replace the diffusion terms by spectral viscosity is straightforward and involves no extra computational load. At each time step the intermediate spectral coefficients $\tilde{\eta}_n^m$, $\tilde{\delta}_n^m$, and $\tilde{\phi}_n'^m$ are found as before, and the spectral viscosity is imposed by finding η_n^m from the implicit equation

$$\eta_n^m = \tilde{\eta}_n^m - 2\Delta t\epsilon\hat{q}_n^2\frac{n^2(n+1)^2}{a^4}\eta_n^m \tag{23}$$

and similarly for $\tilde{\delta}_n^m$ and $\tilde{\phi}_n'^m$. The SV coefficients $\hat{q}_n$ are chosen as in (19), so $\eta_n^m = \tilde{\eta}_n^m$ for $n < n_c$. In particular for $n = 1$ there is no viscous effect and therefore solid-body rotation is undamped. The surface geopotential is included in the $\phi_n'^m$ equation as in (8) to avoid damping due to surface topography.

This implementation of the spectral viscosity may also be written as a filtering operation in spectral space:

$$\eta_n^m = \sigma_n^{\mathrm{SV}}\tilde{\eta}_n^m, \tag{24}$$

$$\sigma_n^{\mathrm{SV}} = \frac{1}{1 + 2\Delta t\epsilon\hat{q}_n^2\dfrac{n^2(n+1)^2}{a^4}}. \tag{25}$$

The filter σ_n^{SV} is plotted in Figs. 1 and 2 (with $M = 42$ and $M = 213$, respectively) for comparison with the standard diffusion filter and the Leith diffusion filter (see section 3c below). The lack of effect of the SV upon lower wavenumbers is reflected by the fact that $\sigma_n^{SV} = 1$ for $n < n_c$.

b. Spectral viscosity parameter tuning

Theoretical considerations yield the scalings (20) for the SV parameters ϵ and n_c. For the numerical calculations in section 4 we set

$$\epsilon = \frac{2a^3}{M^3} \quad \text{and} \quad n_c = 2M^{3/4}. \tag{26}$$

These numerical values were found by demanding good agreement between truncated (lower resolution) kinetic energy spectra and the reference high-resolution spectrum for the single test case described in section 4d (flow over a cylindrical mountain). No further tuning of parameters was performed, yet the SV results are uniformly good across a variety of test problems and truncation values as described in sections 4a and 4b, indicating the universal validity of these parameter values.

c. Diffusion terms based on physical considerations

Although the horizontal diffusion terms (6)–(8) are those used in the current NCAR Community Climate Model (CCM3) and the STSWM test suite code, other global spectral models, for example, at the National Centers for Environmental Prediction, use horizontal diffusion terms that are based upon the work of Leith (1971). Leith examined the numerical dissipation function arising from energy transfer between wavenumbers in a two-dimensional Cartesian turbulence closure model known as the eddy-damped Markovian approximation, under the assumption that a -3 power spectrum is exactly maintained. The resulting dissipation function is close to zero (in fact is slightly negative) for wavenumbers less than approximately 55% of total wavenumber, and rises sharply thereafter. The similarity to the form of the SV term is striking, particularly when it is noted that Leith's derivation is based on physical considerations such as energy cascade within a complex turbulence model, whereas the SV term originated in purely mathematical interest in the discontinuous solutions of nonlinear hyperbolic equations.

We will refer to calculations using the ''Leith diffusion term,'' defined by its implicit implementation:

$$\eta_n^m = \tilde{\eta}_n^m - 2\Delta tK_L\frac{(n-n_L)^2(n-n_L+1)^2}{a^4}\eta_n^m, \tag{27}$$

where n_L is the Leith cutoff wavenumber $n_L = 0.55M$ and the coefficient K_L is related to the artificial diffusion coefficient K_4 by

$$K_L = \begin{cases} 0 & n \le n_L, \\ \dfrac{K_4}{(0.45)^4} & n_L < n \le M. \end{cases} \tag{28}$$

This ensures that the diffusive effect of (27) is close to that of (10) at the highest wavenumbers. The corresponding filter is

$$\eta_n^m = \sigma_n^L\tilde{\eta}_n^m \quad \text{and} \tag{29}$$

$$\sigma_n^L = \frac{1}{1 + 2\Delta tK_L\dfrac{(n-n_L)^2(n-n_L+1)^2}{a^4}}. \tag{30}$$

The coefficient K_4, and so K_L also, decreases like $M^{-2}(M+1)^{-2}$ as the resolution M is increased, in contrast to the M^{-3} decrease of the SV amplitude ϵ. This difference manifests clearly at the high resolution $M = 213$ in Fig. 2.

4. Numerical experiments

The effect of using spectral viscosity or Leith diffusion in place of the artificial diffusion terms in the STSWM is examined in a series of numerical experiments. In section 4a we review some of the test cases from the standard suite proposed by Williamson et al. (1992), concentrating on those cases whose solution

poses a significant challenge to the spectral transform method, namely tests 1, 5, 6, and 7. We show that SV and artificial diffusion both give good results for the height and wind fields when the resolution of the calculation is sufficiently high. In less well-resolved cases, however, we find the SV gives appreciably superior results; three examples of which are presented in section 4b–4d. In all cases the energy spectrum and conservation integrals are more accurate when using SV. Leith's diffusion term has no effect on low wavenumbers and it gives results that are close to the SV results in well-resolved cases. For underresolved cases, however, the SV method gives slightly better energy spectra.

a. Well-resolved test cases

Some of the standard test cases in Williamson et al. (1992) are examined at the resolutions reported in Jakob-Chien et al. (1995); we compare the artificial diffusion results in the latter paper with the corresponding calculations using SV in place of artificial diffusion for four test cases.

1) TEST CASE 1: ADVECTION OF A COSINE BELL

Test case 1 of Williamson et al. (1992) does not deal with the complete shallow water system, but with the simple advection by a constant wind field of a cosine bell height field once around the sphere. The initial height field is given by

$$h(\lambda, \theta) = \begin{cases} 500[1 + \cos(\pi r/R)] & r < R, \\ 0 & r \geq R, \end{cases} \quad (31)$$

where $R = a/3$ and r is the great circle distance between (λ, θ) and the center $(3\pi/2, 0)$. This height field should be recovered exactly after one rotation (288 h). As the advection equation is linear, no steepening of the height field or cascade of energy occurs. For this reason the artificial diffusion terms F_η, F_δ, and F_ϕ were set to zero in Jakob-Chien et al. (1995) for this test case. The spectral transform solution with $M = 42$ (denoted T42 hereafter, for triangular truncation of order 42) is quite satisfactory, except for small ripples in the region where the solution ought to be uniformly zero. These ripples are due to the discontinuity in the second derivative of (31) at the base of the cosine bell, and can be eliminated by postprocessing (see Gottlieb and Shu 1998; Gelb and Tadmor 2000). Figures 3a and 3b show cross sections of the height field, taken along constant longitude $\lambda = 3\pi/2$ and constant latitude (closest grid point to) $\theta = 0$ after one rotation. The direction parameter is $\alpha = \pi/2$ here, so the bell is advected directly over the poles, demonstrating the lack of a ''pole problem'' in spectral methods. Next, the spectral viscosity terms (14)–(16) were included in the calculation in order to check for excessive diffusion. The cross sections are displayed in Figs. 3c and 3d. The similarity of this case to the zero diffusion solution is in contrast to the effect of the artificial diffusion terms (6)–(8): when these are included the maximum of the height field is clearly eroded (Figs. 3e and 3f), with corresponding effects upon the global L_2 error norm (Fig. 4). We note that the ripples to the north of the bell are slightly larger in the SV case than when using artificial diffusion; this is due to the retention of more high-wavenumber information by the SV term, which permits the use of high-resolution reconstruction methods (see, e.g., Fig. 13). The smearing can also be avoided by using the Leith diffusion term (Figs. 3g and 3h). In fact for most of the well-resolved test cases, the spectral viscosity and Leith diffusion terms have almost identical effects, and so we hereafter present only the SV results unless the Leith diffusion case is substantially different. The similarity reflects the fact that in these test cases the dominant scales of motion are very well resolved (i.e., with active wavenumbers n less than the cutoffs n_c and n_L) and so do not feel diffusive effects.

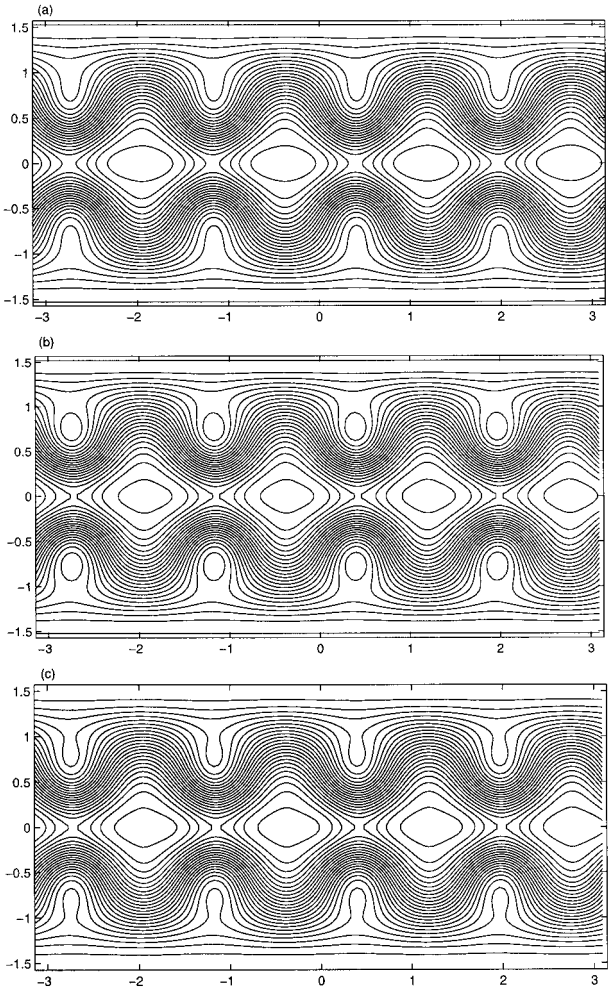

FIG. 9. Height field for day 14 of test case 6: (a) T213 reference, (b) T42 artificial diffusion, and (c) T42 spectral viscosity. Contours are from 8100 to 10 500 m at 100-m intervals.

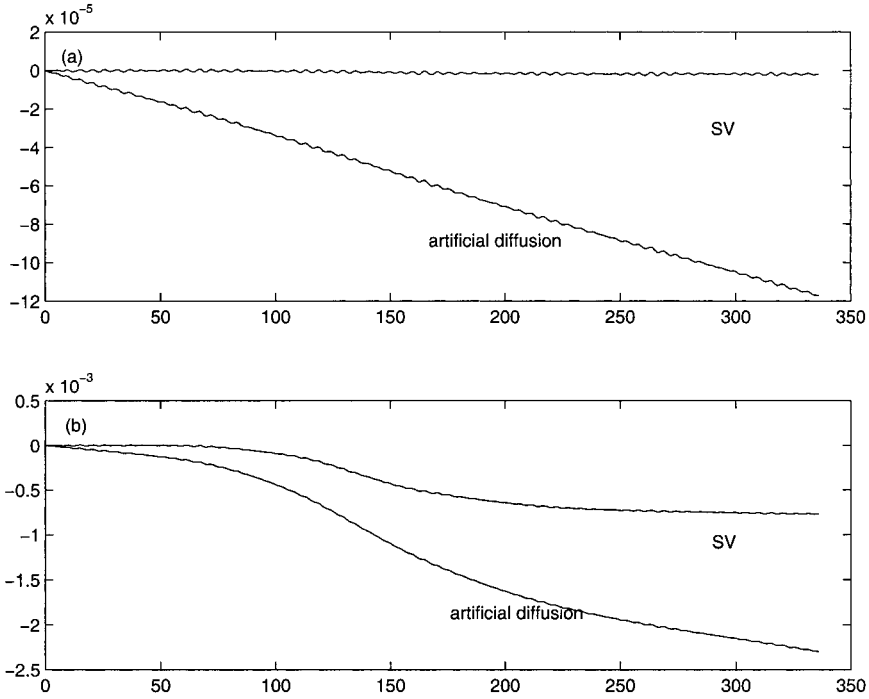

FIG. 10. Global conservation integrals for T42 test case 6, using artificial diffusion and spectral viscosity: (a) normalized total energy and (b) normalized potential enstrophy.

2) TEST CASE 5: FLOW OVER A CONICAL MOUNTAIN

The initial conditions for test case 5 consist of a zonal flow impinging upon a conical mountain of radius $R = \pi/9$ and height $h_{s_0} = 2000$ m centered at $\lambda_c = 3\pi/2$, $\theta_c = \pi/6$. The surface geopotential is thus given by

$$\phi_s = gh_{s_0}(1 - r/R), \tag{32}$$

with $r^2 = \min[R^2, (\lambda - \lambda_c)^2 + (\theta - \theta_c)^2]$. As no analytic solution exists, a high-resolution (T213) calculation is used to provide a reference solution. With the exception of some spectral representation problems near the mountain, the T42 calculation in Jakob-Chien et al. (1995) using artificial diffusion gives results that are reasonably close to the reference solution. In Fig. 5 we compare the height field at day 15 for the T42 artificial diffusion and SV cases, with global L_2 error norm in Fig. 6. These indicate comparable accuracy of SV and artifical diffusion in this well-resolved case. However, improved accuracy of the SV case is apparent when examining the conservation of global energy and potential enstrophy in Fig. 7, and the kinetic energy spectrum in Fig. 8. Note the energy is conserved to five digits when using artificial diffusion but to seven digits with spectral viscosity, which is approaching the limits of machine accuracy. The potential enstrophy is conserved to one extra digit. Conservation of global mass, divergence, and vorticity are chiefly influenced by machine accuracy, and do not display significant differences between the artificial diffusion and SV cases.

3) TEST CASE 6: ROSSBY–HAURWITZ WAVE

Test case 6 evolves a wavenumber-4 Rossby–Haurwitz wave initial condition over 14 days; see Williamson et al. (1992) for details of initial condition and Jakob-Chien et al. (1995) for time step restrictions in this case. A T213 reference calculation of the height field at day 14 is presented in Fig. 9a, along with the T42 solution using artificial diffusion and SV (Figs. 9b and 9c, respectively). Again, the height field is similar in both cases with the SV case slightly closer to the reference solution. The total energy is better conserved by SV (to six digits, compared to four digits with artificial diffusion), as is the potential enstrophy (Fig. 10). In common with the previous case, no noticeable differences are apparent between SV and artificial diffusion cases in the conservation of mass, vorticity, or divergence.

4) TEST CASE 7: ANALYZED 500-MB INITIAL CONDITIONS

The analyzed atmospheric conditions of 21 December 1978 are used as initial conditions in test case 7, and evolved forward to day 5. We present the kinetic energy spectra on day 5 in Fig. 11. Once more we find the SV result is appreciably better than the artificial diffusion case with the T42 SV spectrum being much closer to the ''true'' spectrum provided by the T213 reference solution. Differences are less apparent in the height fields (Fig. 12): although spectral viscosity better re-

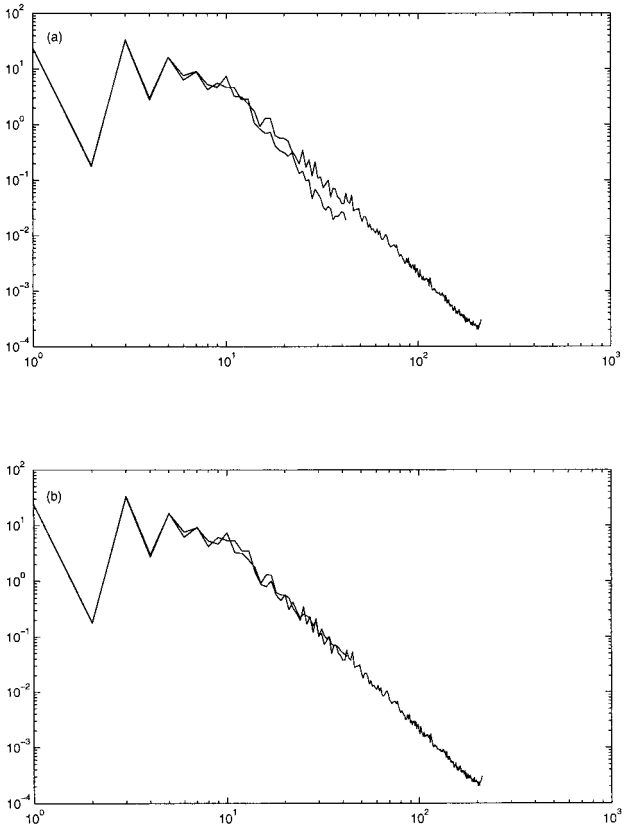

FIG. 11. Kinetic energy spectra for day 5 of test case 7: (a) T213 reference solution and T42 artificial diffusion and (b) T213 reference solution and T42 spectral viscosity.

solves the low over the Yukon, both it and the artificial diffusion fail to resolve the low over Britain and Ireland.

b. Advection of a cylinder

More dramatic differences among the effects of SV, Leith diffusion, and artificial diffusion become evident when the problem cannot be well-resolved using the available computational power. As a simple example we replace the cosine bell height field of test case 1 by a cylinder:

$$h(\lambda, \theta) = \begin{cases} 1000 & r < R, \\ 0 & r \geq R, \end{cases}$$

with r and R as before. The exact solution after one rotation is again equal to the initial condition. This discontinuous field poses significant representational problems for the spectral basis and, as expected, the diffusion terms have nontrivial effects. The cross sections of the height field after one revolution with artificial diffusion are shown in Figs. 13a and 13b. The smearing effect of the artificial diffusion is very evident here, and clearly the information on the location of the edges of the cylinder has been lost. By contrast, the SV solution (Figs. 13c and 13d) retains the edge information at the cost

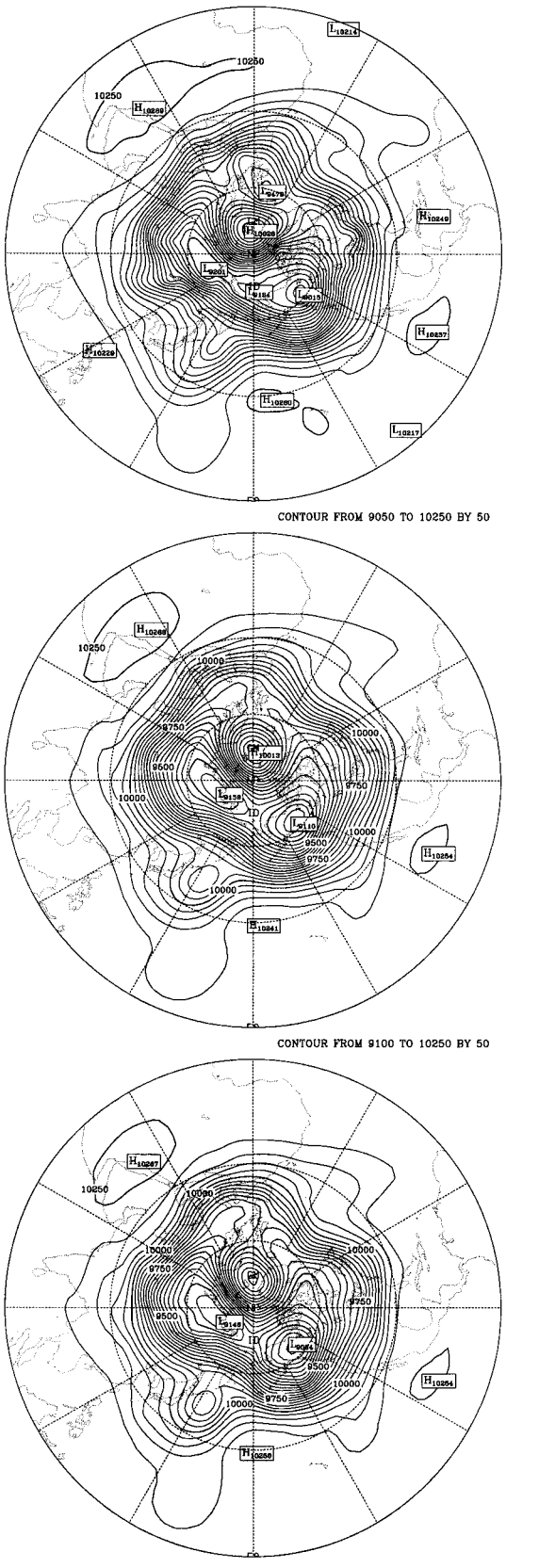

FIG. 12. Height field for day 5 of test case 7, north polar stereographic projection: (a) T213 reference, (b) artificial diffusion, and (c) spectral viscosity.

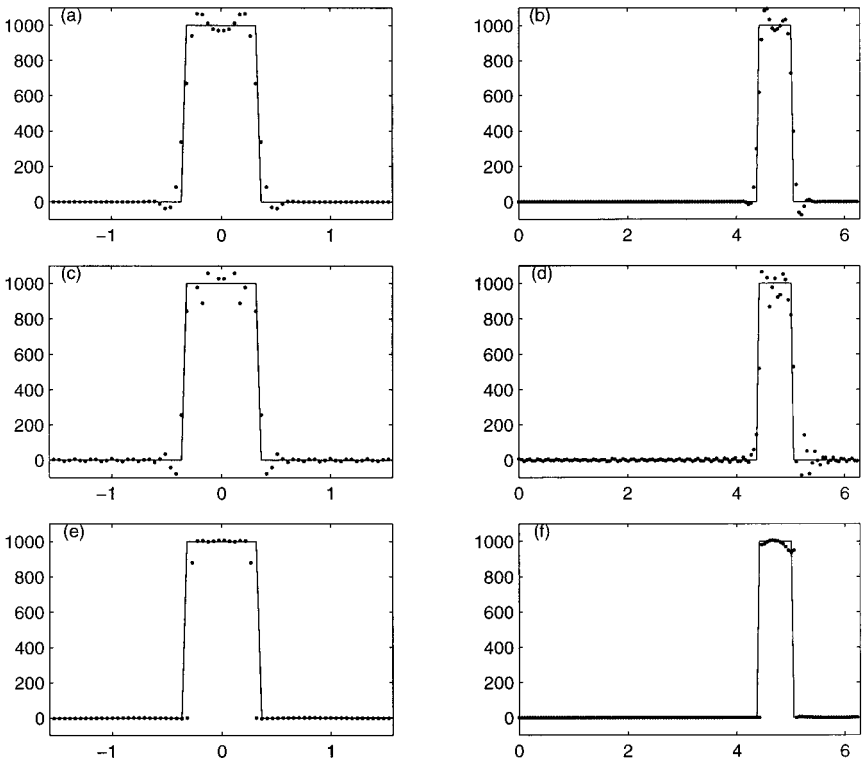

FIG. 13. Exact (solid line) and numerical (dots) height field for T42 advection of cylinder after one rotation with $\alpha = 0$: (a), (b) artificial diffusion, (c), (d) spectral viscosity, and (e), (f) postprocessed solution obtained from SV. Constant longitude cross sections on left and constant latitude on right.

of less reduction of the Gibbs oscillations. The edge information is critical in postprocessing methods that both recover correct height values and significantly reduce the Gibbs oscillations.

As an example of such methods, we apply a Gegenbauer reconstruction method to the SV solution in Figs. 13e and 13f. The algorithm successfully detects the discontinuities and reconstructs the solution using a two-dimensional version of the Gegenbauer method (Gottlieb and Shu 1998). Note the elimination of the ripples in the smooth parts of the solution, as well as the lack of Gibbs oscillations, which are still evident in the artificial diffusion case.

c. *Underresolved flow over conical mountain*

To further examine the problems associated with smearing when spectral resolution is relatively low, we return to test case 5 as outlined in section 4a(2), but calculate at T10 rather than T42 as before. With low resolution the numerical method cannot be expected to give good approximations to the reference solution (Fig. 5a), but it is hoped that the main large-scale flow features can be at least crudely distinguished. With this in mind, we examine the day 15 forecasts from the artificial diffusion calculation (Fig. 14a) and spectral viscosity case (Fig. 14b). The artificial diffusion coefficient K_4 used is consistent with the $[M(M + 1)]^{-2}$ scaling advocated in Jakob-Chien et al. (1995). As expected, the height field has large errors close to the mountain, but the basic structure of the reference solution is emerging in Fig. 14b. On the other hand, the artificial diffusion case clearly demonstrates the excessive smearing effect, especially notable in the Southern Hemisphere, where almost all of the finer-scale structure has been lost. Since the cutoff wavenumber n_c given by (26) is greater than M in this case, the SV case is equivalent to using no diffusion term at all. In other words, the parameter choice (26) effectively ''turns off'' the diffusive action when the number of modes is so small that diffusion leads to less accurate results. An alternative choice for the SV cutoff, for example $n_c = 0.75M$ (without changing ϵ), activates SV on the highest 25% of modes but, as shown in Fig. 14c, is still more accurate than the artificial diffusion case. The Leith diffusion results are very similar to the SV case and so are not shown.

d. *Flow over a cylindrical mountain*

While the previous example used a rather extreme case of low resolution to highlight the improvement of the SV over the artificial diffusion, the behavior seen there is typical of what happens when resources do not permit full resolution of the flow. If the problem is suf-

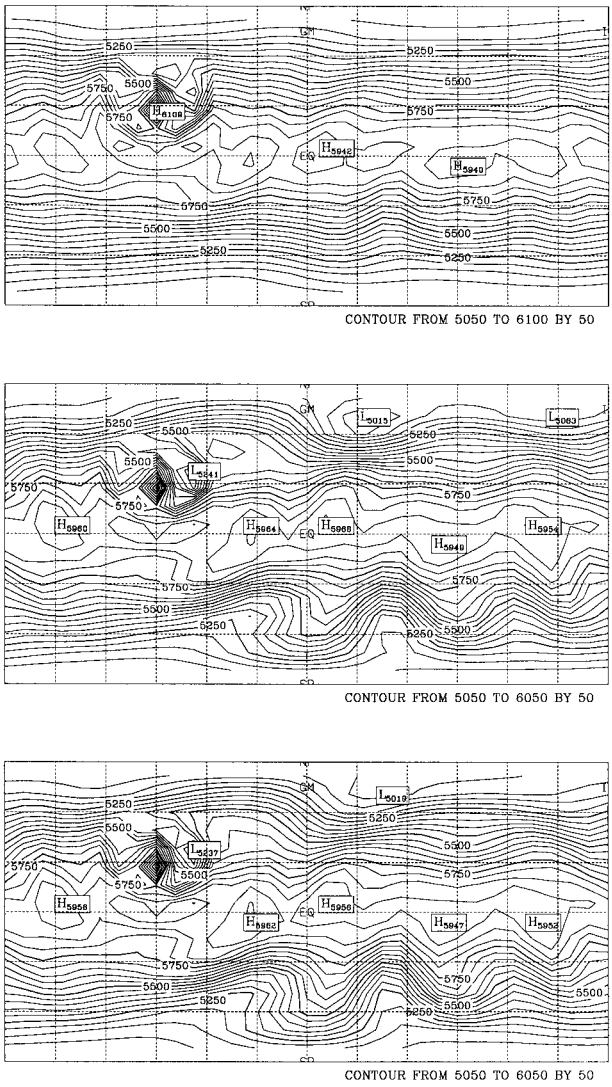

FIG. 14. T10 height field for flow over a conical mountain: (a) artificial diffusion, (b) spectral viscosity with $n_c > M$, and (c) spectral viscosity with $n_c = 0.75M$.

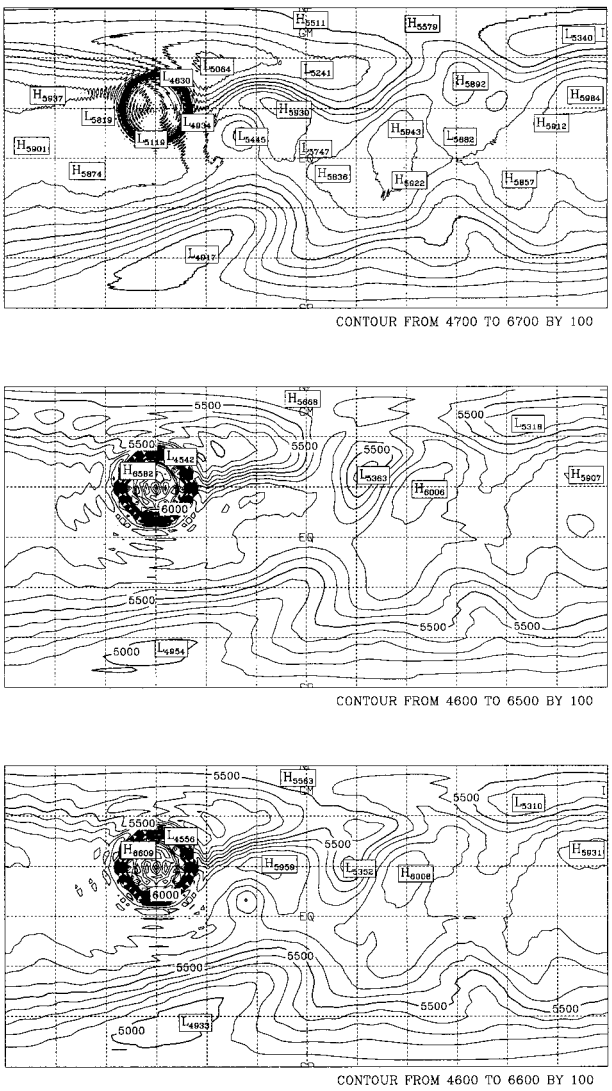

FIG. 15. Height field for day 15 of flow over a cylindrical mountain: (a) T213 reference (with artificial diffusion), (b) T42 artificial diffusion, and (c) T42 spectral viscosity.

ficiently complex, then even at more realistic resolutions the undesirable effects of the artificial diffusion are manifest. We consider once more the initial conditions of test case 5, but now modify the surface topography from a conical [as in Eq. (32)] to a cylindrical mountain:

$$\phi_s = \begin{cases} gh_{s_0} & r < R, \\ 0 & r \geq R, \end{cases}$$

with r, R, and h_{s_0} defined as in section 4a(2). Clearly the spectral representation of this discontinuous surface will be less accurate than for the conical mountain that was continuous. We again present results at day 15 and use a T213 calculation as the reference solution. The height field contains some spectral ringing even at T213 (Fig. 15a), and without a diffusion or SV term becomes spectrally blocked. This is clear from the turnups in the tail of the energy spectrum; see Fig. 16. The Leith diffusion, SV, and artificial diffusion cases have more realistic spectra and are almost identical for wavenumbers less than 100. Note that the SV case has the least turnup at the highest wavenumbers.

At a working resolution of T42 the kinetic energy spectrum for the four cases of (a) no diffusion, (b) artificial diffusion, (c) spectral viscosity, and (d) Leith diffusion are presented in Fig. 17. Adding diffusion cures the spectral blocking, with artificial diffusion being overdiffusive and SV being somewhat more accurate than the Leith diffusion case. The height predictions of the T42 artificial diffusion (Fig. 15b), T42 spectral viscosity (Fig. 15c) and the T213 reference solution (Fig. 15a) all clearly show the representational problems at the cylindrical mountain. Although the artificial diffu-

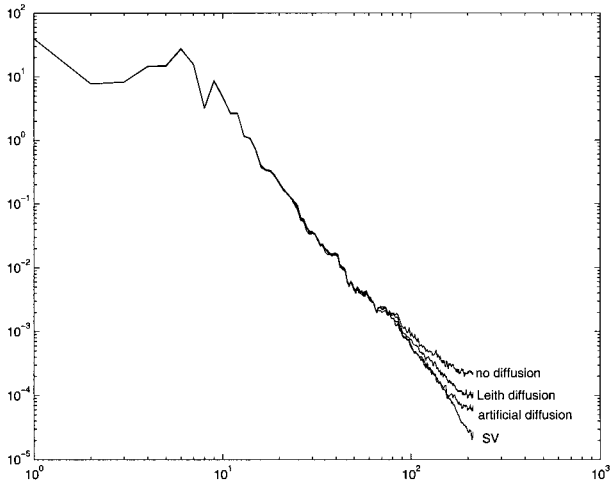

FIG. 16. Kinetic energy spectra for day 15 T213 flow over a cylindrical mountain using various diffusion terms.

sion case is not obviously smeared, a number of important flow details are better predicted by the SV. Of particular interest in the flow behind (east of) the mountain, where the reference solution shows the height contours shifted to the north, with a high of 5930 m directly east of the mountain and a low of 5445 m offset to the southwest of the high. Although the T42 approximation is naturally cruder, these features are well represented in the SV case, but are absent in the artificial diffusion plot. The importance of accurately predicting these features is underlined by the wind vector plots in Fig. 18. The cyclone and anticyclone to the east of the mountain (at $\lambda \sim 5\pi/6$ or longitude 30°W) are correctly positioned in the SV plot, with an east-southeasterly flow between them, in contrast to the inaccurate positions and east-northeasterly separating flow in the artificial diffusion case.

5. Conclusions

The numerical experiments reported in section 4 present compelling evidence for the superiority of a spectral viscosity term over the standard diffusion terms in the shallow water spectral transform model of Jakob-Chien et al. (and as employed in the NCAR CCM3 global spectral model). Unlike subgrid mixing models, the SV term is based not on physical arguments, but rather on a rigorous mathematical approach to the problems exhibited at large wavenumbers in truncated spectral models. The theory underlying the spectral viscosity method

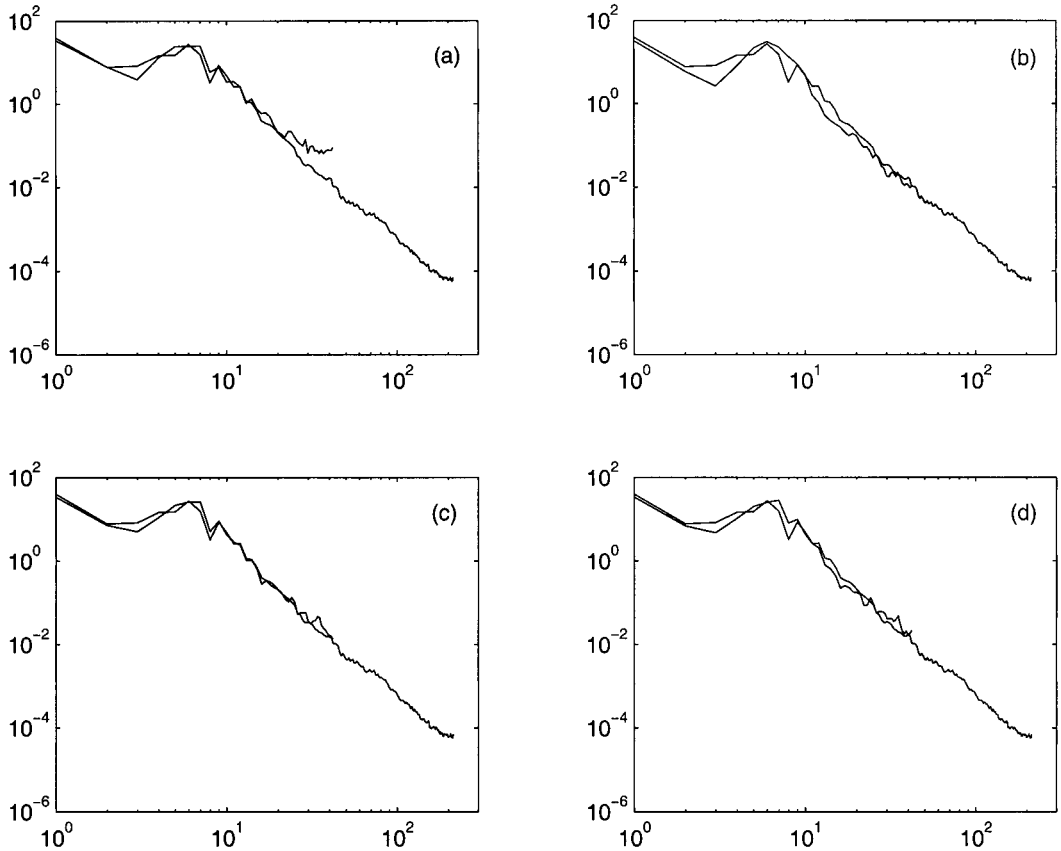

FIG. 17. Kinetic energy spectra for T42 flow over a cylindrical mountain, compared to T213 reference spectrum: (a) no diffusion, (b) artificial diffusion, (c) spectral viscosity, and (d) Leith diffusion.

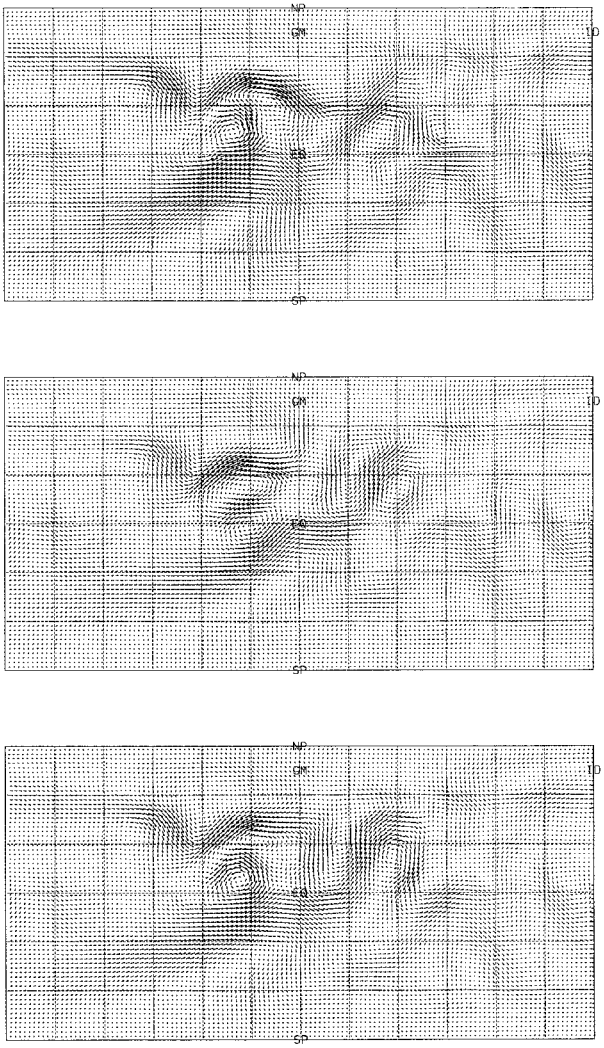

FIG. 18. Wind vectors for day 15 of flow over a cylindrical mountain: (a) T213 reference solution (with artificial diffusion) projected onto T42, (b) T42 artificial diffusion, and (c) T42 spectral viscosity.

provides the scalings (20) of the SV parameters ϵ and n_c; the only free parameters are their numerical coefficients. We stress again that these were tuned for a single test case, all other test cases then used these values. The advantages of the SV over the artificial diffusion may be summarized as follows: 1) less smearing of height and wind fields, which permits use of high-resolution postprocessing methods; 2) improved resolution of spectral blocking problem, and 3) more accurate numerical conservation of invariants. These advantages are similar to those found when using a diffusion term based on the work of Leith (1971). Similar results were found using SV and Leith diffusion in most cases, with the SV yielding slightly improved energy spectra when the flow is underresolved or resolution is high. Leith's method is based on physical considerations, in contrast to the mathematical theory underlying the SV ideas. This implies that the SV approach is suitable for more general problems where a detailed physical analysis such as Leith's is not available. It is suggested that the SV theory presented here may also be helpful when choosing parameters in models that already employ a Leith diffusive term. For example, the Leith cutoff wavenumber $n_L = 0.55M$ can easily be altered to the SV cutoff $n_c = 2M^{3/4}$, and similarly the coefficient K_L can be related to the SV amplitude ϵ. Finally it is noted that the SV terms are very simply implemented in existing spectral transform models, with no extra computational cost. We believe that application to three-dimensional global atmospheric models will yield comparably favorable results.

Acknowledgments. This research was supported in part by a Sloan Foundation Fellowship (AG), the Fulbright Commission (JPG), and the System Science and Engineering Research Center at ASU. Assistance provided by John Truesdale, David Williamson, and Jim Hack with NCAR's STSWM computer code and documentation is gratefully acknowledged.

APPENDIX

Derivation of Spectral Viscosity Term

We wish to extend the ideas of Tadmor (1989), Tadmor (1993), and Ma (1998) to derive a spectral viscosity term on the sphere. In fact, as the standard diffusion term (6) is fourth order, we use a superviscosity (also known as hyperviscosity) form of the SV for comparison, but for clarity will first concentrate here on a regular (second order) viscosity.

The SV term for the one-dimensional conservation law

$$\frac{\partial}{\partial t}u + \frac{\partial}{\partial x}f(u) = 0 \tag{A1}$$

is defined by analogy with the concept of weak formulations of (A1), which are known to yield physically correct entropy solutions. The SV term is derived by demanding that for test functions ψ

$$\left[\frac{\partial}{\partial t}u + \frac{\partial}{\partial x}f(u),\, \psi\right] = \epsilon\left[\frac{\partial}{\partial x}(Qu), \frac{\partial}{\partial x}(Q\psi)\right] + (B(u),\, \psi),$$

where the parentheses denote a suitable inner product and $B(u)$ is a penalty operator that enforces the boundary conditions. Following integration by parts and noting that Q is self-adjoint with respect to the inner product, the SV equation (away from boundaries) is

$$\frac{\partial}{\partial t}u + \frac{\partial}{\partial x}f(u) = -\epsilon Q\frac{\partial^2}{\partial x \partial x}(Qu),$$

and boundary terms must be included at end points.

In order to define a spherical SV term for, say, the vorticity equation (3),

$$\frac{\partial \eta}{\partial t} = -\frac{1}{a(1-\mu^2)}\frac{\partial}{\partial \lambda}(U\eta) - \frac{1}{a}\frac{\partial}{\partial \mu}(V\eta),$$

we proceed by analogy with the method described above. Introducing a test function ψ on the sphere and a suitable inner product, we demand that

$$\left[\frac{\partial \eta}{\partial t} + \frac{1}{a(1-\mu^2)}\frac{\partial}{\partial \lambda}(U\eta) + \frac{1}{a}\frac{\partial}{\partial \mu}(V\eta),\ \psi\right] = \epsilon[\nabla(Q\eta),\ \nabla(Q\psi)].$$

Here the one-dimensional derivative has been generalized to its simplest multidimensional equivalent, and Q is assumed to be isotropic, that is, defined as in Eq. (17). Noting the vector identity

$$\nabla(Q\eta)\cdot\nabla(Q\psi) = \nabla\cdot[\nabla(Q\eta)Q\psi] - \nabla^2(Q\eta)Q\psi$$

and using the divergence theorem on the sphere yields

$$\left[\frac{\partial \eta}{\partial t} + \frac{1}{a(1-\mu^2)}\frac{\partial}{\partial \lambda}(U\eta) + \frac{1}{a}\frac{\partial}{\partial \mu}(V\eta),\ \psi\right] = -\epsilon[\nabla^2(Q\eta),\ Q\psi].$$

In contrast to the one-dimensional case, no boundary terms appear as the sphere is a closed surface. As before Q is self adjoint with respect to the inner product, and so we derive

$$\frac{\partial \eta}{\partial t} = -\frac{1}{a(1-\mu^2)}\frac{\partial}{\partial \lambda}(U\eta) - \frac{1}{a}\frac{\partial}{\partial \mu}(V\eta) - \epsilon Q\nabla^2(Q\eta),$$

and the final term on the right-hand side is the desired SV term. The extension to a super-SV term is relatively straightforward (see Ma 1998) and yields the equation

$$\frac{\partial \eta}{\partial t} = -\frac{1}{a(1-\mu^2)}\frac{\partial}{\partial \lambda}(U\eta) - \frac{1}{a}\frac{\partial}{\partial \mu}(V\eta) - \epsilon Q\nabla^4(Q\eta), \tag{A2}$$

giving the SV term (14). As the SV operator is isotropic, we adopt the one-dimensional scalings for the cutoff and amplitude given by Eq. (20).

This derivation is rather intuitive and the extension of the convergence results of Tadmor (1989) is, as yet, unproven. Nevertheless, computational results are very encouraging and lead us to propose the super-SV term as a viable alternative to standard artificial diffusion terms.

REFERENCES

Andreassen, O., I. Lie, and C. E. Wasberg, 1994: The spectral viscosity method applied to simulation of waves in a stratified atmosphere. *J. Comput. Phys.,* **110,** 257–273.

Bourke, W., B. McAvaney, K. Puri, and R. Thurling, 1977: Global modeling of atmospheric flow by spectral methods. *Methods Comput. Phys.,* **17,** 267–324.

Canuto, C., M. Y. Hussaini, A. Quarteroni, and T. A. Zang, 1987: *Spectral Methods in Fluid Dynamics.* Springer-Verlag, 600 pp.

Chen, G.-Q., Q. Du, and E. Tadmor, 1993: Spectral viscosity approximations to multidimensional scalar conservation laws. *Math. Comput.,* **61,** 629–643.

Eliasen, E., B. Machenbauer, and E. Rasmussen, 1970: On a numerical method for integration of the hydrodynamical equations with a spectral representation of the horizontal fields. Institut for Teoretisk Meteorologi Rep. 2, University of Copenhagen, 35 pp.

Gelb, A., and E. Tadmor, 2000: Enhanced spectral viscosity approximations for conservation laws. *Appl. Numer. Math.,* **33,** 3–21.

Gottelmann, J., 1999: A spline collocation scheme for the spherical shallow water equations. *J. Comput. Phys.,* **148,** 291–298.

Gottlieb, D., and C.-W. Shu, 1998: On the Gibbs phenomenon and its resolution. *SIAM Rev.,* **39,** 644–668.

Hack, J. J., 1992: Climate system simulation. *Climate System Modeling,* K. E. Trenberth, Ed., Cambridge University Press, 283–318.

——, and R. Jakob, 1992: Description of a shallow water model based on the spectral transform method. NCAR Tech. Note NCAR/TN-342+STR, 39 pp. [NTIS PB92-155258.]

Jakob, R., J. J. Hack, and D. L. Williamson, 1993: Solutions to the shallow water test set using the spectral transform method. NCAR Tech. Note NCAR/TN-388+STR, 82 pp. [NTIS PB93-202729.]

Jakob-Chien, R., J. J. Hack, and D. L. Williamson, 1995: Spectral transform solutions to the shallow water test set. *J. Comput. Phys.,* **119,** 164–187.

Karamanos, G.-S., and G. E. Karniadakis, 1999: A spectral vanishing viscosity method for large eddy simulations. *J. Comput. Phys.,* **163,** 22–50.

Leith, C. E., 1971: Atmospheric predictability and two-dimensional turbulence. *J. Atmos. Sci.,* **28,** 145–161.

Lesieur, M., and O. Metais, 1996: New trends in large-eddy simulations of turbulence. *Annu. Rev. Fluid. Mech.,* **28,** 45–82.

Ma, H.-P., 1998: Chebyshev–Legendre super spectral viscosity method for nonlinear conservation laws. *SIAM J. Numer. Anal.,* **35,** 893–908.

Maday, Y., and E. Tadmor, 1989: Analysis of the spectral vanishing viscosity method for periodic conservation laws. *SIAM J. Numer. Anal.,* **26,** 854–870.

——, S. M. Ould Kaber, and E. Tadmor, 1993: Legendre pseudospectral viscosity method for nonlinear conservation laws. *SIAM J. Numer. Anal.,* **30,** 321–342.

Orszag, S. A., 1970: Transform method for calculation of vector coupled sums: Application to the spectral form of the vorticity equation. *J. Atmos. Sci.,* **27,** 890–895.

——, 1974: Fourier series on spheres. *Mon. Wea. Rev.,* **102,** 56–75.

Robert, A. J., 1966: The integration of a low-order spectral form of the primitive meteorological equations. *J. Meteor. Soc. Japan,* **44,** 237–244.

Spotz, W. F., M. A. Taylor, and P. N. Swarztrauber, 1998: Fast shallow-water solvers in latitude–longitude coordinates. *J. Comput. Phys.,* **145,** 432–444.

Swarztrauber, P. N., 1996: Spectral transform methods for solving the shallow-water equations on the sphere. *Mon. Wea. Rev.,* **124,** 730–744.

Tadmor, E., 1989: Convergence of spectral methods for nonlinear conservation laws. *SIAM J. Numer. Anal.,* **26,** 30–44.

——, 1993: Super viscosity and spectral approximations of nonlinear conservation laws. *Numerical Methods for Fluid Dynamics IV,* M. J. Baines and K. W. Morton, Eds., Clarendon Press, 69–82.

Taylor, M., J. Tribbia, and M. Iskandarani, 1997: The spectral element method for the shallow water equations on the sphere. *J. Comput. Phys.,* **130,** 92–108.

Williamson, D. L., J. B. Drake, J. J. Hack, R. Jakob, and P. N. Swarztrauber, 1992: A standard test set for numerical approximations to the shallow water equations in spherical geometry. *J. Comput. Phys.,* **102,** 211–224.